Design of a XYZ Scanner For Home-made High-speed Atomic Force Microscopy

Kunhai Cai[1,2], Xianbin He[1], Yanling Tian[1*,2], Xianping Liu[2], Dawei Zhang[1], Bijan Shirinzadeh[3]

[1]Key Laboratory of Mechanism Theory and Equipment Design of Ministry of Education, Tianjin University, Tianjin 300072, China

[2]School of Engineering, University of Warwick, Coventry CV4 7AL, UK

[3]Robotics and Mechatronics Research Laboratory, Department of Mechanical and Aerospace Engineering, Monash University, Clayton, VIC 3800, Australia

Abstract—Atomic force microscopy (AFM) is a useful tool in nanoscale measurement. However, conventional AFM suffers from slow scan speed, limiting the use for biological detection or nanofabrication, due to the limited bandwidth of AFM components. In which the resonant frequency of the AFM scanner is usually too low to achieve high-speed scanning. In this paper, a simple and compact home-made high-speed AFM is set up and reported. As an important part of the scanning system, a parallel kinematic piezoelectric actuator (PZT) XYZ scanner is proposed, which can achieve high bandwidth and low coupling errors. Finite element analysis (FEA) is adopted to characterize the scanner, and verified the first two lateral resonance frequency of 5.6 kHz and the vertical resonance frequency is 29 kHz. In addition, some testing experiments are implemented, demonstrating feasibility of the proposed scanner. Finally, it was applied to the home-made AFM system, and some effective scanning imaging results can be obtained.

Keywords — AFM scanner, Parallel kinematic, High-speed AFM, Scanning

I. Introduction

Since the creation of atomic force microscopy, the method to measure and manipulate materials in nanoscale is enriched a lot [1, 2]. Unlike the use of scanning

electron microscopy (SEM) or scanning tunnel microscopy (STM), AFM obtain the morphology of the sample by 'touching' the surface with intermolecular force, making it possible to scan in air, vacuum or liquid. However, a traditional AFM system suffers from the limitation of slow scanning rate, it means that would take a large amount of time to complete an image. For example, a commercial AFM would take more than 2 minutes to obtain a 128 × 128 pixels resolution image with a typical scan rate of 1 Hz [3], which is too slow for biological detection [4, 5] nanofabrication [6, 7]. It is well know that high-speed operation of an AFM are increasingly required, and it is also a challenge for the researchers. There are three main limiting factors include: the resonant frequency of the AFM cantilever, the speed of the data processing system and the bandwidth of scanner [8, 9]. Some small-sized and high bandwidth cantilevers were proposed for fast-scanning [10, 11]. Field-Programmable Gate Array (FPGA) and rapid acquisition system were used to implement the required controller and data processing. As a very important part of AFM system, scanner will have a significant impact the result of the scanning imaging and operation. Conventionally, piezoelectric tube scanners are the most widely used scanner in commercial AFMs, because it has excellent resolution, simple structure, easy to install and configure. However, it has two fatal flaws include: the low resonance frequency and apparent cross coupling error, which seriously affected the scanning rate and reduced the imaging accuracy of AFM. Therefore, it should be search another scanner to replace the conventional piezoelectric tube, one have high resonance frequencies and accuracy.

In recent years, design of a novel scanner for HS-AFM has aroused people's interest. The idea is to improve its resonant frequency based on flexible hinge structure. Several XYZ nanopositioning scanners have been reported [12-14], which consists of a XY stage and a Z stage. A number of commercial AFMs have appeared in the market, which were equipped with flexure-based nanopositioning platforms [15, 16]. Flexure-guided mechanisms are categorized into two main configurations: serial or parallel. Depending on design requirements, some configurations have been reported. For serial kinematic mechanism, such as, Leang and Fleming [17] presented a

serial-kinematic two-axis (XY) high-speed scanner in 2009. And a XYZ AFM scanner was presented by Kim et al [18]. Wadikhaye et al [19] presented a compact serial-kinematic XYZ scanner in 2011. The next year, another serial-kinematic high-performance XYZ stage was reported by Kenton and Leang [20], which was integrated with a commercial AFM. In addition, for another flexure mechanism: parallel kinematic mechanism, Yong et al [21] design of a high-speed nanopositioner based on parallel flexure-guided mechanism. A novel scanner presented by Schitteret al [22], which enables scanning speeds three orders of magnitude faster than the conventional AFMs. Klapeteket al [23] presented a scanning system enables generating nano-resolution and over mm^2 regions. Li et al [24] design, analysis, and testing of a parallel-kinematic high-bandwidth XY stage driven by PZTs. Due to parallel structures offer high motion accuracy and mechanical stiffness, leading to high resonance frequencies and compactness, parallel flexure-guided mechanism are increasingly utilized in high-speed nanopositioning stages.

In this paper, we proposed a parallel kinematic high-speed piezoelectric actuator (PZT) XYZ scanner. High resonance frequencies and low cross-coupling errors are our design goals. The scanner consists of a parallel kinematic XY stage and a Z stage. The Z stage is mounted on the central moving platform of the XY stage. To achieve the design objective, several parallel leaf flexure hinge mechanisms are designed in two orthogonal symmetrical directions, and around the central moving platform of the XY stage. Symmetrical leaf flexure is arranged radially evenly on the Z stage, is adopted to achieve high resonance frequencies and decoupling. Then, finite element analysis (FEA) is utilized to validate the characteristics of the scanner. And some testing experiments are conducted, demonstrating feasibility of the proposed scanner. Finally, it was applied to a home-made AFM system, which is the first time we build and report. And some scanning imaging results were obtained.

This paper is organized as follows. Section II describes the design and characterization of the parallel kinematic XYZ scanner. Section III presents the testing experiment of the scanner while section IV shows the home-made AFM system and

scanning imaging obtain by applying the proposed scanner. Section V concludes the paper.

II. Mechanical Design and Model Verification

A. Mechanical design

This paper presented an AFM scanner, which consists of a XY stage, a Z stage, three piezoelectric actuators (PZTs). The assembly view of the scanner is shown in Fig. 1.

In this section, the mechanical design of XYZ scanner is aimed at achieving high resonance frequencies and low cross-coupling errors. Therefore, based on parallel mechanism design ideas, the proposed XY stage as shown in Fig. 2(a), the central moving platform (where the Z stage is attached) is connected to four link units through four parallel flexure mechanisms (two leaf-spring hinges), and four link units are connected to the frame through another eight parallel flexure mechanisms (two leaf-spring hinges). Due to orthogonally symmetrical structural design, the identical kinematic flexure hinge mechanisms in X and Y axes guarantee the uniform characteristics of the central moving platform, in other words, the scanner behavior in the X and Y -axis are the same, for example, when the PZT is activated in the Y direction, the parallel leaf flexure mechanisms transmits the motion to the central moving platform due to its high longitudinal rigidity (is highlighted in dashed lines in Fig. 2(a)); while another parallel leaf flexure mechanisms function as a prismatic joint due to their low transverse stiffness in the orthogonal direction. The same principle movement of the scanner in the X-axis can be speculated.

As shown in Fig. 2(b), the Z stage is also designed with the parallel flexure mechanisms, which can be fixed with four bolts on the moving platform. The end-effector is connected to the fix frame through four leaf-spring hinges. Four leaf-spring hinges are located at the same circle with the separation angle of 90°, therefore, when the Z-axis PZT is activated, the end-effector can only moves along the Z direction without cross-axis coupling errors.

Benefiting from the above design, when the scanner is applied to an AFM system, the end-effector can be used to carry a sample, and it can move along in the X, Y and Z directions to meet the needs of scanning.

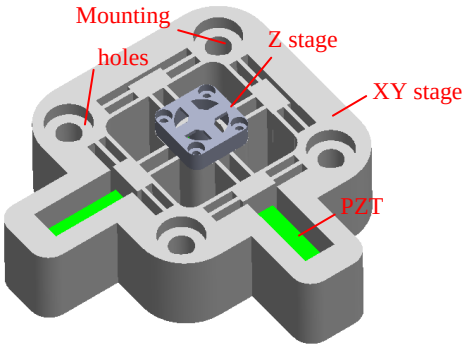

Figure 1 3D solid model of the scanner.

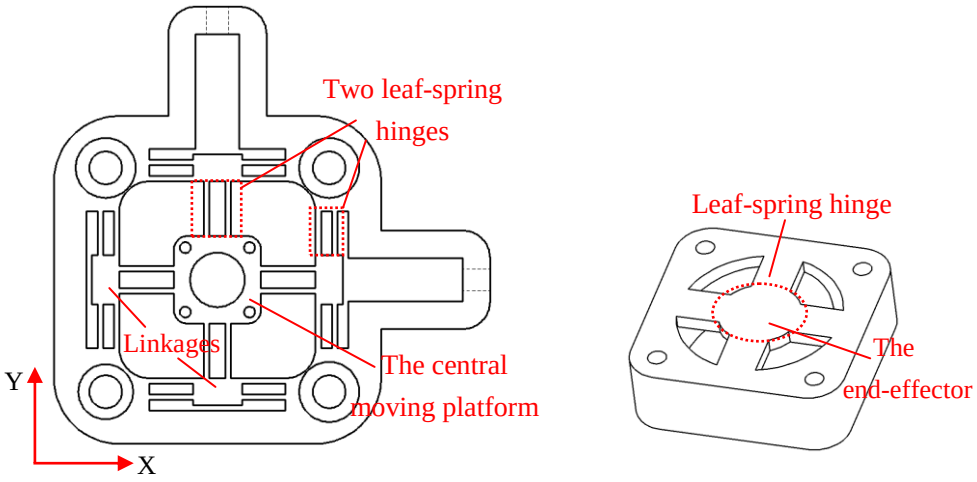

(a) XY stage (b) Z stage

Figure 2 2D model of the scanner.

B. Model verification

In this section, in order to validate the design model and obtain further insights into the static and dynamic characteristics of the developed XYZ scanner, the commercial finite element software ANSYS is utilized to perform the simulation analyses. The material for the scanner is chosen as Aluminum 7075-T6 with a density of 2770 kg/m3, a Young's modulus of 71GPa, and a Poisson's ratio of 0.33. Both of the XY and Z stages are bonded together. In order to improve the computational accuracy, the

mapping mesh method is adopted. The mesh is strictly controlled in the areas of flexure hinges, where the large deformation is generally occurred.

In order to observe the motion characteristics of the scanner, the static characteristic analysis is carried out. For the designed goals, the in-plane stiffness of the scanner should be higher, which can be improved the rejection capability against external disturbances. After the simulation analysis, the linear stiffness without PZTs installed can be obtained, 25.63, 25.72 and 10N/μm in the X, Y and Z direction, respectively. In addition, an out-of-plane stiffness is also a key factor in determining its capacity of resisting disturbance. In this scanner, the out-of-plane stiffness of 222 N/μm is achieved.

The dynamic characteristics of the scanner are need to focus on, and the simulation results are shown in Fig. 2. The first two mode shape are moved along the X- and Y-axis with the frequency of 5684.9 Hz and 5688.5 Hz, respectively; the third and fourth mode shape rotate and moved along the Z-axis, with the corresponding frequencies of 14471 Hz and 29464 Hz, respectively. This result confirms the first lateral resonance frequency of 5.6 kHz that is about six times higher than traditional piezoelectric tube scanners. It means that the scanner has better dynamic characteristic.

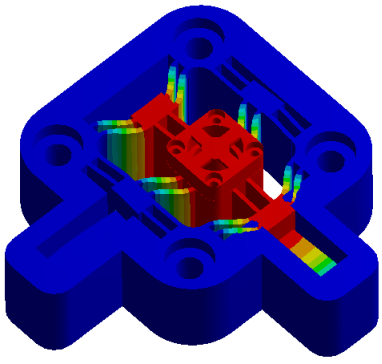

(1st) 5684.9 Hz

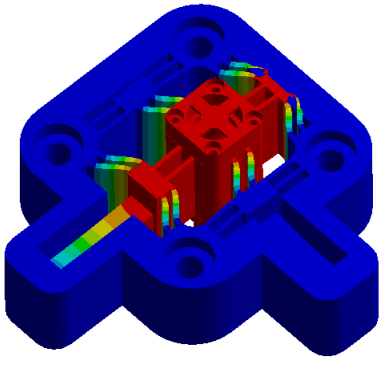

(2nd) 5688.5 Hz

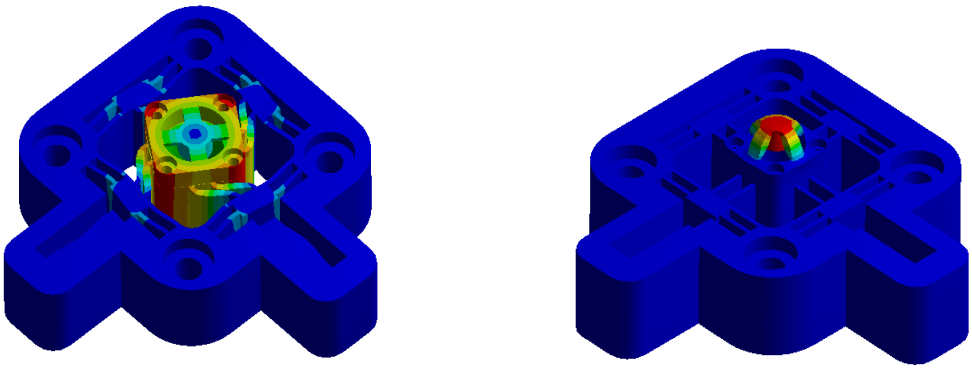

(3rd) 14471 Hz (4st) 29464 Hz

Fig. 3 First four modal of the scanner.

III. Testing of the Scanner

The developed prototype of the scanner is shown in Fig. 4. The top and bottom surfaces are fabricated on a milling machine, respectively. Subsequently, artificial aging is utilized to release the residual stress. Computer numerical control (CNC) assisted wire electrical discharge the machining (WEDM) technique is utilized to manufacture all the flexure structures. During the WEDM fabrication process, low-speed feeding is selected to guarantee the machining accuracy, and a fabrication tolerance of 2 μm is achieved. Both of the XY and Z stages are bolted together.

The performance of the proposed scanner was systematically evaluated. As shown in Fig. 5, the scanner is actuated by three THORlabs (PZS001 6 mm × 7 mm × 20 mm) piezoelectric stack actuators which are driven by the THORlabs (MDT693A) voltage amplifier with the gain of 7.5~15. There are four strain gauges placed on each of the actuator to form a full Wheatstone bridge. The strain of the actuator is measured by the strain gauge and processed with Dynamic Strain Gauges (SDY2105). Three PI (D510.021) single-electrode capacitive sensors with a measurement range of 20 μm and a resolution of 0.2 nm were used to capture the motions of the scanner before being amplified by a PI (E-509.E03) amplifier. The mounting direction of the sensor is shown in Fig. 5. The control signal of the motions and the data acquisition task are implemented using a NI motion control card (PCI-7344) and USB-6251. And the

whole experiments finished on a Newport RS-4000 optical table so as to reduce the external disturbances.

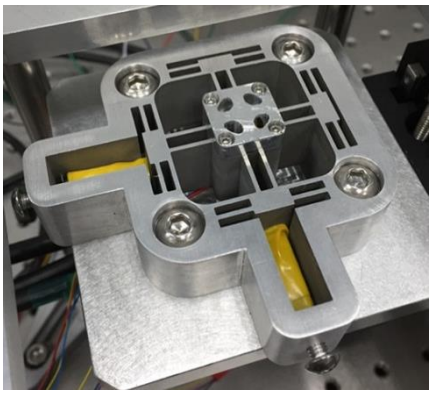

Figure 4 The developed prototype of the scanner

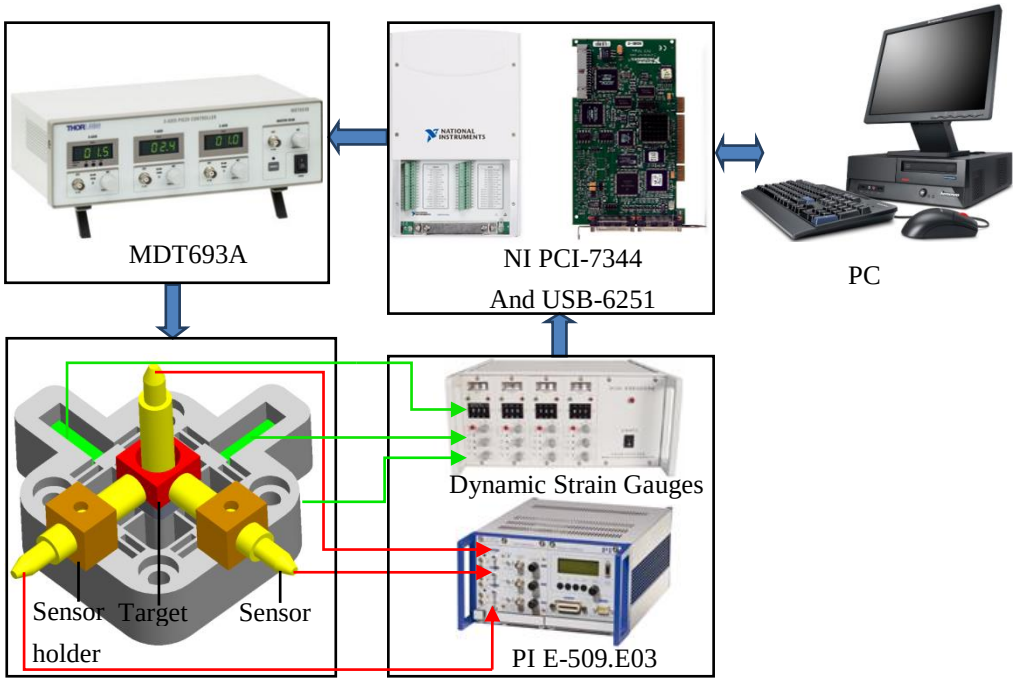

Figure 5 The schematic diagram of testing control

A. Motion range and coupling error

In order to validate the effective motion range of the scanner, by applying a 1 Hz sawtooth voltage signal to each PZT, and the maximum displacement in three working axes are measured. A motion range of 8.7 μm is achieved in the X direction as shown in Fig. 6(a), meanwhile, the induced parasitic motion in Y- and Z-axis are depicted, respectively. Similarly, the measure result in Y-axis is shown in Fig. 6(b),

and it reveal that the maximum crosstalk is 0.12 μm in X-axis and 0.1 μm in Z-axis, which are about 1.2% and 1.03% of the primary Y-axis motion, respectively. In addition, the end-effector can reach 10.6 μm movement displacements in the Z direction as shown in Fig. 6(c), the coupled errors in the X- and Y- directions are 0.2346 μm and 0.2752 μm (0.88% in the X axis, 0.39% in the Y axis), respectively. These errors are mainly due to the assembly errors, manufacture errors.

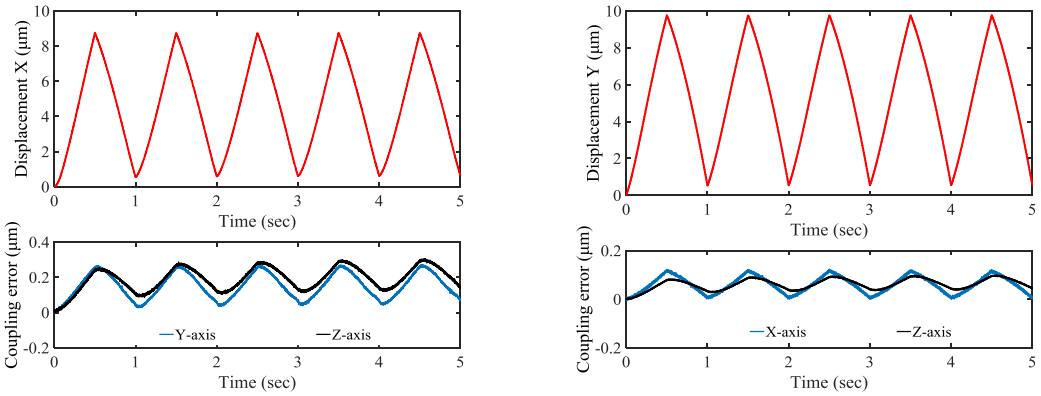

(a) X-axis (b) Y-axis

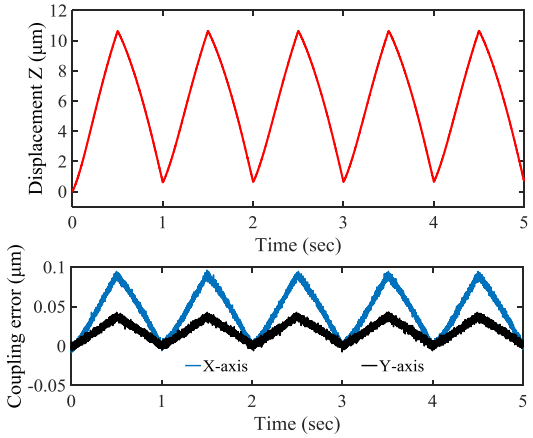

(c) Z-axis

Figure 6 The result of motion range

B. Resolution

As shown in Fig. 7, precision information are also tested and verified. The resolution in three directions of the scanner are clearly observed from the multi-step response experiment, which as regards three stability measures are 9 nm in the X-axis, 8 nm in the Y-axis and 8 nm in the Z-axis, respectively.

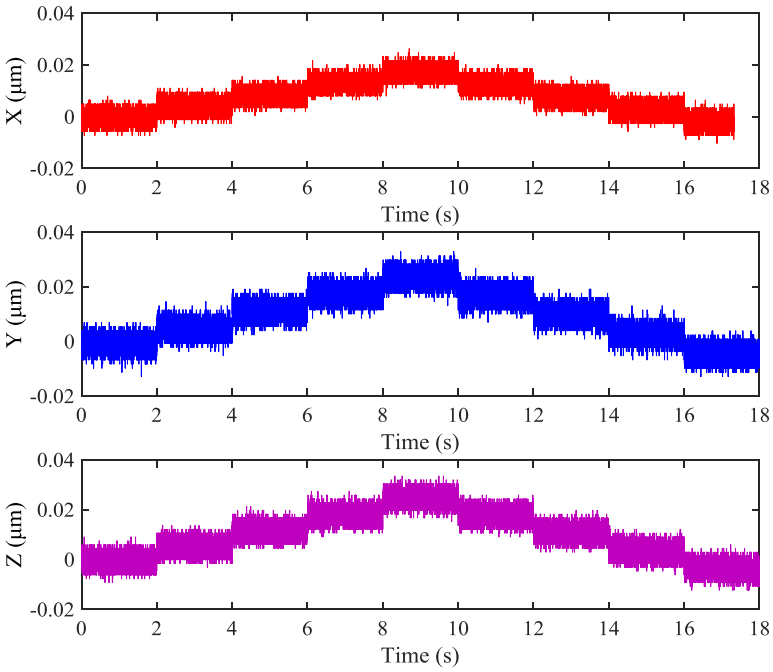

Figure 7 The result of resolution

C. Trajectory tracking

In order to overcome the positioning error is caused by the hysteresis and nonlinear of PZTs. The inverse Bouc-Wen model can be cascaded to the physical system as a feedforward hysteresis compensator, which is designed to reduce the tracking error problem and improve the positioning accuracy of the scanner. It has already been verified that the Bouc-Wen model is suitable for compensating for hysteresis errors of PZT [25, 26]. The tracking results of the scanner with hysteresis compensation are shown in Fig. 8, 9 and 10, respectively. The maximum tracking error of the 3-axes scanner is below 2% at the frequency of 10Hz, and below 3% at the frequency of 20Hz.

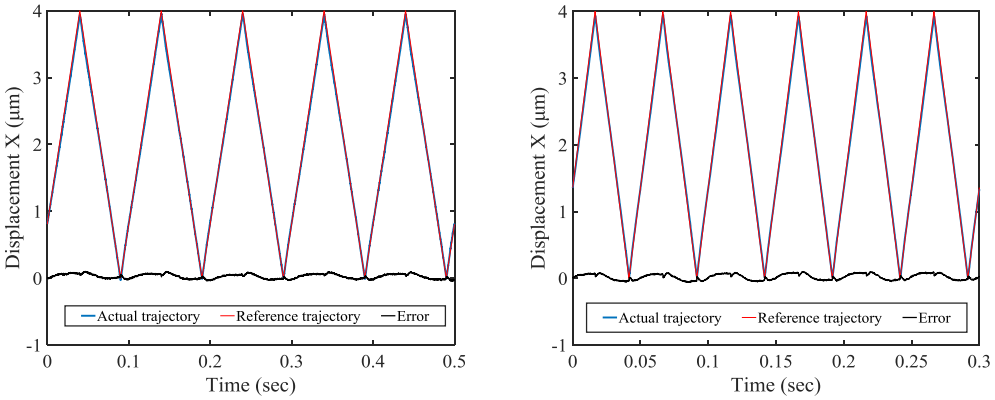

(a) 10Hz (b) 20Hz

Figure 8 Tracking result of the X-axis

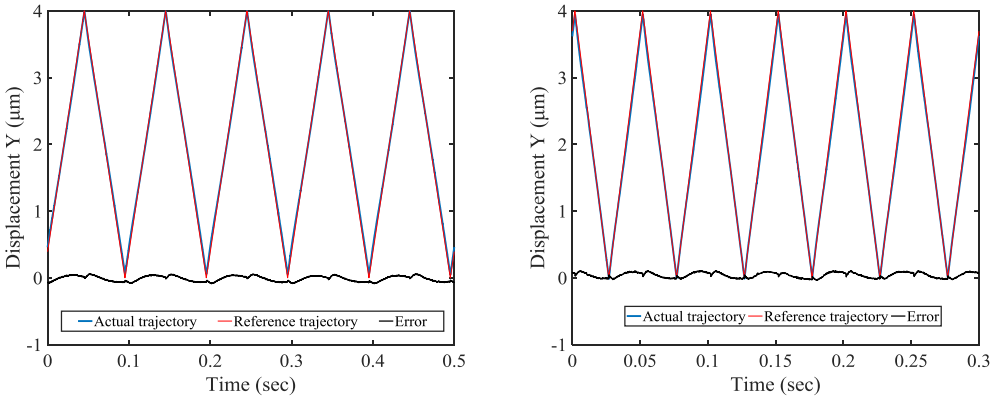

(a) 10Hz (b) 20Hz

Figure 9 Tracking result of the Y-axis

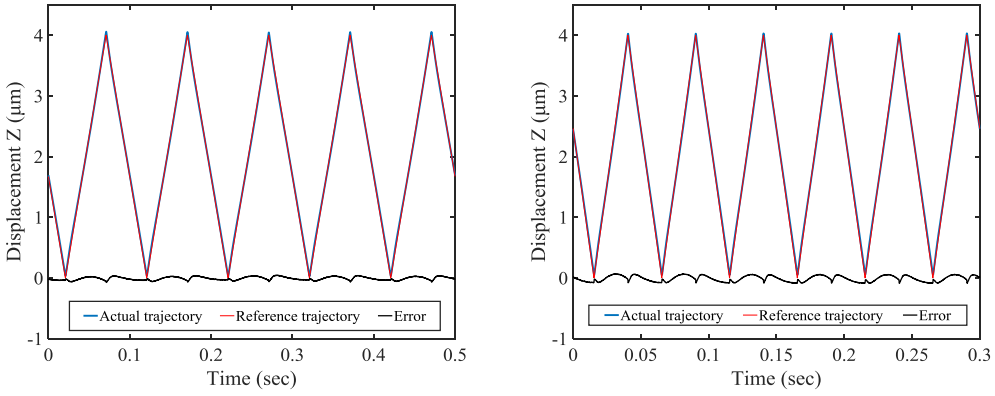

(a) 10Hz (b) 20Hz

Figure 10 Tracking result of the Z-axis

IV. The Home-made AFM System

In this section, the implementation of the AFM system is discussed. The block diagram and experimental setup of the home-made system are shown in Fig. 11 and Fig. 12. As stated in our previous testing, the strain signals, which are received and processed by the NI data acquisition card (USB-6251), act as the lateral sensors of the nanopositioner. The tip-sample force is maintained by the close-loop between the position sensitive detector (PSD) signal and the vertical driving voltage of the piezoelectric stack actuator. The close-loop motion is achieved by the slave controller NI motion control card (PCI-7344). Three micropositioners are arranged perpendicular to each other to fast bringing the sample to the AFM probe.

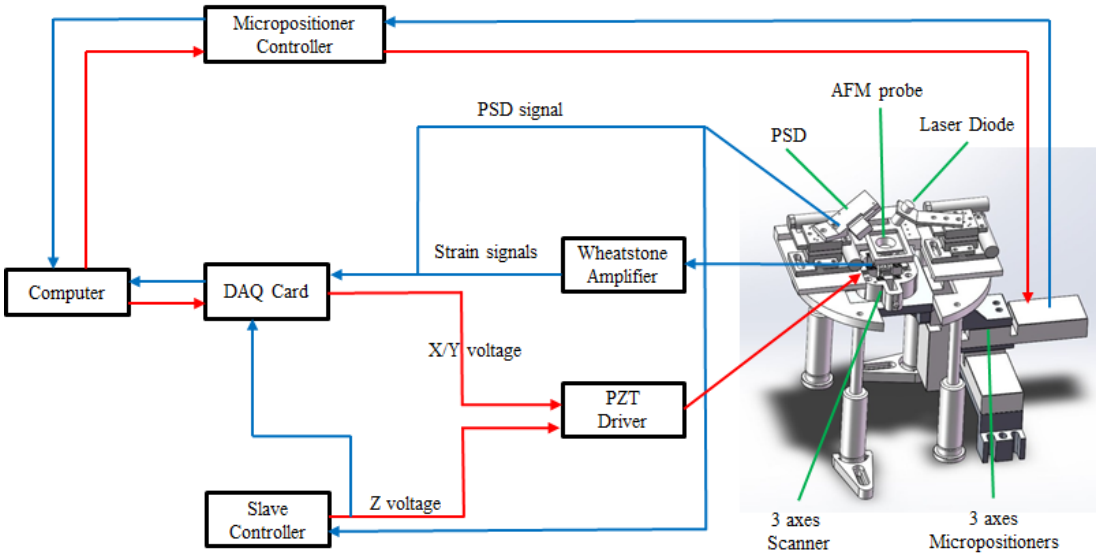

Figure 11 Block diagram of the home-made AFM system

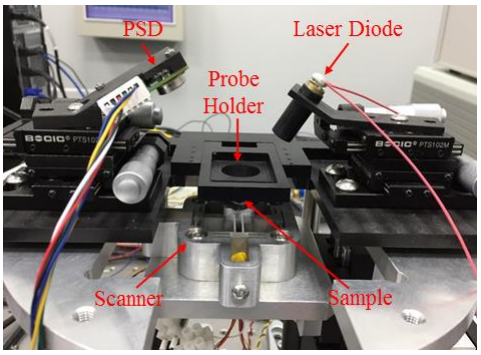

Figure 12 Experimental setup of the AFM head and scanner.

A. Calibration of the AFM System

In order to obtain the height of the sample, the relationship between the control voltage of the vertical (Z-axis) piezoelectric stack actuator and the deformation of cantilever should be clarified. A standard grating (MikroMasch TGZ2) with nominal depth value of 108nm is scanned slowly with feedback control in the Z-axis. In this case, the photo-diode error signal is extremely small; hence, the static gain can be directly calculated from the control voltage. After repeated testing and plenty of data analysis, the control signal is taken as 0.175V corresponding with a 108nm grating. Therefore, the static gain *k* can be determined as:

$$k = \frac{108}{0.175} = 616(nm/V) \tag{1}$$

B. Motion Coupling Compensation

According to the previous testing, the coupling motion in Z axis is inevitable when driving PZT in the X axis or Y axis (due to machining and installation errors). In order to reduce the coupling error, one simple method is to compensate the Z-axis according to the X displacement and Y displacement. It can be expressed as:

$$z' = z - (\alpha \cdot x + \beta \cdot y) \tag{2}$$

where *z* represents the displacement of the Z-axis, *z'* is the value after compensation, respectively, α and β are fitting parameters.

C. Imaging Performance

In HS-AFM, the time, which the AFM probe stays for at each pixel point, is too short for the tip to become stable. Therefore, during constant force scanning, PSD signal is combined to compensate the error of the vertical driving voltage:

$$H = k \cdot (\pm U_z + \frac{U_{PSD}}{k_1}) \tag{3}$$

Where U_z is the driving voltage in the Z axis which is needed for the AFM tip to track the sample surface in constant force mode, its polarity is decided according to the structure of the AFM scanner: U_z is positive in tip-scanning based AFM scanner and negative in sample-scanning based AFM scanner, U_{PSD} is the PSD feedback voltage, k_1 is the ratio between the input Z voltage and the output PSD voltage in open-loop, the PSD is about 0.33 V corresponding to 1 V excitation signal.

The performance of our home-made AFM system is validated by scanning a standard grating sample. A MikroMasch TGZ2 calibration grating with 3 μm period and 108 nm step height was scanned, which was mounted on the scanner and raster-scanned with pure triangular waveforms at 1 Hz, 10 Hz and 25 Hz, respectively. Scans were performed using a BudgetSensors ContAl cantilever probe with a first resonance frequency of 13 kHz and a stiffness of 0.2 N/m.

Fig.13 shows the imaging performance of the home-made AFM system. An area of 7 μm × 8 μm of the grating was imaged at line rates of 1, 10, and 25 Hz at pixel resolution of 512 ×512. During raster scanning (X axis is the fast axis while Y axis the slow axis), there is no distortion in the images at different scanning speed, and have a very similar quality. However, a slightly difference can be observed due to open-loop compensation scanning, and the scanning speed is limited to 25 Hz with the resolution of 512 × 512 pixels since the slaved motion controller PCI-7344 has only 16 kHz sampling rate. Therefore, close-loop scanning and slave controller with faster sampling rate are needed in our future research.

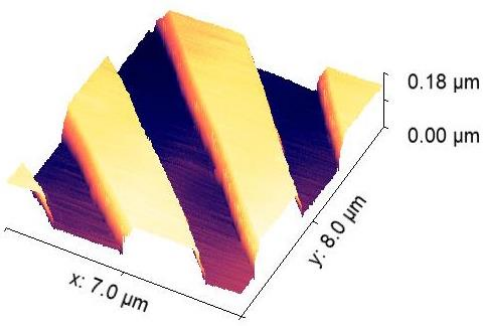

(a) 1 Hz

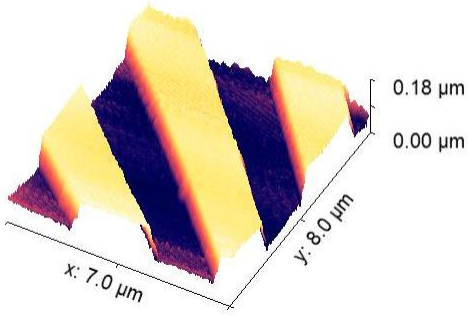

(b) 10 Hz

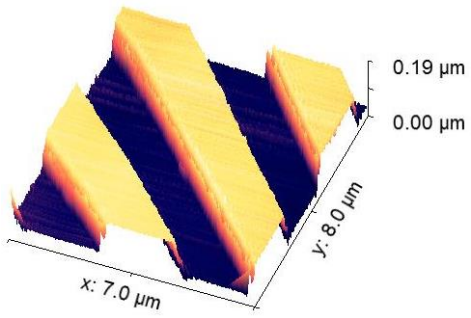

(c) 25 Hz

Figure 13 The scanning results of the home-made AFM

V. Conclusions

In this paper, design of a novel high-bandwidth piezoelectric actuator (PZT) AFM scanner based on parallel kinematic. The scanner consists of a parallel kinematic XY stage and a Z stage. Then, finite-element analysis (FEA) is utilized to validate the static and dynamic characteristics of the proposed scanner, the first resonant modes at 5.6 kHz along both the X- and Y-axes, and 29 kHz along the Z-axis can be obtained, which ensures that the system has good dynamic characteristic. In addition, some testing experiments were implemented, confirming feasibility of the proposed scanner. Finally, it was applied to the home-made AFM system, and some effective scanning imaging results can be obtained by scanning of standard gratings with the scan speed up to 25 Hz, the resolution of the image is 512 × 512 pixels. The results showed that the scanner is well qualified for high-speed scanning. Further research will focus on implementing faster control board and data acquisition system in order to rate up the scan speed.

Acknowledgment

This work was supported by the National Natural Science Foundation of China (No. 51505330, 51675371, 51420105007), EU H2020 MSCA RISE 2016 (No.734174) and China Scholarship Council (Grant No. 201606250048).

References

[1] G. Binnig, H. Rohrer, Ch. Gerber, and E. Weibe, “Surface studies by scanning tunneling microscopy”, Phys. Rev. Lett., pp. 49:57, 1982.

[2] G. Binnig, C. F. Quate, and Ch. Gerber, “Atomic force microscope”, Phys. Rev. Lett., pp. 56:930, 1986.

[3] Y. K. Yong, S. O. R. Moheimani, “Collocated z-axis control of a high-speed nanopositioner for video-rate atomic force microscopy”, IEEE T. Nanotechnol., vol. 14 (2), pp. 338-345, 2015.

[4] T. Ando, T. Uchihashi, N. Kodera, “High-speed atomic force microscopy for observing dynamic biomolecular processes”, J. Mol. Recognit., vol. 20(6), pp. 448-458, 2007.

[5] T. Ando, T. Uchihashi, N. Kodera, “High-speed afm and nano-visualization of biomolecular processes”, Pflug. Archeur. J. Phy., vol. 456(1), pp. 211-225, 2008.

[6] A. A. Tseng, “Advancements and challenges in development of atomic force microscopy for nanofabrication”, Nano Today., vol. 6(5), pp. 493-509, 2011.

[7] J. A. Vicary, M. J. Miles, “Real-time nanofabrication with high-speed atomic force microscopy”, Nanotechnol., vol. 20(9), pp. 95302, 2009.

[8] T. Ando, “High-speed atomic force microscopy coming of age”, Nanotechnol., vol. 23(6), pp. 62001, 2012.

[9] G. Schitter, K. J. Astrom, B. E. DeMartini, “Design and modeling of a high-speed afm-scanner”, IEEE T. Contr. Syst. T., vol.15(5), pp. 906-915, 2007.

[10] M. Kitazawa, K. Shiotani, and A. Toda, “Batch Fabrication of Sharpened Silicon Nitride Tips,” Jpn. J. Appl. Phys., vol. 42, pp. 4844–4847, 2003.

[11] J. D. Adams, B. W. Erickson, J. Grossenbacher, J. Brugger, A. Nievergelt, and G. E. Fantner, “Harnessing the damping properties of materials for high-speed atomic force microscopy,” Nat. Nanotechnol. , vol. in press, pp. 1–6, 2015.

[12] Asylum research, see http://asylumresearch.com for information on flexure-based nanopositioning platforms.

[13] Park Systems, see www.parkafm.com for information on the use of flexure-based nanopositioning platforms in commercially available AFMs.

[14] T. Ando, N. Kodera, D. Maruyama, E. Takai, K. Saito, and A. Toda, “A high-Speed atomic force microscope for studying biological macromolecules in action,” Jpn. J. Appl. Phys., vol. 41, no. 7B, pp. 4851-4856, 2002.

[15] G. Schitter, K. J. Astrom, B. DeMartini, P. J. Thurner, K. L. Turner, and P. K. Hansma, "Design and modeling of a high-speed AFM-scanner," IEEE Trans. Contr. Syst. Tech., vol. 15, no. 5, pp. 906-915, 2007.

[16] Y. K. Yong and S. O. R. Moheimani, "Design, modeling, and FPAA-based control of a high-speed atomic force microscope nanopositioner," IEEE/ASME Trans. Mechatron., vol. 18, no. 3, pp. 1060-1071, 2013.

[17] K. K. Leang and A. J. Fleming, "High-speed serial-kinematic SPM scanner: Design and drive consideration," Asian J. Control, vol. 11, No. 2, pp. 144-153, 2009.

[18] D. Kim, D. Kang, J. Shim, I. Song, D. Gweon, "Optimal design of a flexure hinge-based XYZ atomic force microscopy scanner for minimizing Abbe errors," Rev. Sci. Instrum., vol. 76, no. 7, pp. 1-6, 2005.

[19] S.P. Wadikhaye, Y.K. Yong, S.O.R. Moheimani, "Design of a compact serial-kinematic scanner for high-speed atomic force microscopy: an analytical approach," Micro Nano Lett., vol. 7, no. 4, pp. 309-313, 2012.

[20] B. Kenton and K. Leang, "Design and control of a three-axis serial-kinematic high-bandwidth nanopositioner," IEEE/ASME Trans. Mechatron., vol. 17, no. 2, pp. 356-369, 2012.

[21] Y. K. Yong, S. O. R. Moheimani, "Collocated Z-Axis Control of a High-Speed Nanopositioner for Video-Rate Atomic Force Microscopy," IEEE Trans. Nanotechnol., vol. 14, no. 2, pp. 338-345, 2015.

[22] G. Schitter, P. J. Thurner, P. K. Hansma, "Design and input-shaping control of a novel scanner for high-speed atomic force microscopy," Mechatronics, vol. 18, no. 5-6, pp. 282-288, 2008.

[23] P. Klapetek, M. Valtr, L. Picco, O. D. Payton, J. Martinek, A. Yacoot and M. Miles, "Large area high-speed metrology SPM system," Nanotechnology, vol. 26, no. 6, pp. 1-9, 2015.

[24] C. X. Li, G. Y. Gu, M. J. Yang and L. M. Zhu, "Design, analysis and testing of a parallel-kinematic high-bandwidth XY nanopositioning stage," Rev. Sci. Instrum., vol. 84, no. 12, pp. 1-12, 2013.

[25] K. Cai, Y. Tian, F. Wang, D. Zhang, X. Liu, B. Shirinzadeh, Modeling and tracking control of a novel XY theta Z stage, Microsys. Technol., vol. 23(8), pp. 3575-3588, 2017.

[26] K. Cai, Y. Tian, F. Wang, D. Zhang, B. Shirinzadeh, Design and Control of a 6-degrees-of-freedom Precision Positioning System, Robot. Cim-Int. Manuf., vol. 44, pp. 77-96, 2017.